nature communications

Article

https://doi.org/10.1038/s41467-024-55726-5

Two dimensional confinement induced discontinuous chain transitions for augmented electrocaloric cooling

Received: 26 December 2023

Accepted: 23 December 2024

Published online: 15 January 2025

Check for updates

Fang Wang[1], Zhong-Ye Wang[2], Yao-Rong Luo[3], Ming-Ding Li[1,4], Yu-Rong Yang[3], Wei Li[2], Xiao-Liang Wang[1], Tiannan Yang[5] ✉ & Qun-Dong Shen[1] ✉

Overheating remains a major barrier to chip miniaturization, leading to device malfunction. Addressing the urgent need for thermal management promotes the development of solid-state electrocaloric cooling. However, enhancing passive heat dissipation through two-dimensional materials in electrocaloric polymers typically compromises the electrocaloric effect. In this work, we utilize two-dimensional polyamide with porous structure and hydrogen bonding to achieve multiple polar conformations with short-range order in the electrocaloric composite polymers. The structure minimizes intermolecular interactions while reducing energy barriers for field-driven polar-nonpolar conformational transitions. The electrocaloric polymer exhibits doubled cooling efficiency at electric fields as low as 40 MV m^{-1}. Additionally, the electrode design achieves a vertical deformation of 2 millimeters, demonstrating the feasibility of self-driven electric refrigeration devices. This porous organic two-dimensional material resolves cooling efficiency limitations from spatial confinement, advancing the integration of two-dimensional materials in flexible electronics.

With the advancement of mobile devices and integrated circuits, the issue of overheating caused by high power consumption is becoming increasingly severe[1]. Overheated central processors (CPUs) may fail directly or be forced to reduce performance as self-protective measures are activated to counteract thermal strain[2]. To prevent a reduction in operating frequency and maintain device efficiency, heat dissipation must be accelerated. In recent years, solid-state cooling technology based on electrocaloric effect (ECE) has attracted great attention due to its advantages of flexibility, ease of miniaturized integration, and free from global-warming-potential refrigerants[3,4]. What's more, these devices require only electrical energy for both driving and cooling processes. Based on electrocaloric materials, various thermal management devices can be developed, including lattice type, cascade flow type, and self-powered type[5–9]. Compared with traditional heat dissipation methods, these solid-state refrigeration devices exhibit superior performance in terms of lightweight and cooling efficiency. This technology shows great potential for application in integrated circuits, helping to mitigate performance degradation caused by overheating and enhancing user experience.

[1]Department of Polymer Science and Engineering, Key Laboratory of High-Performance Polymer Materials and Technology of MOE, State Key Laboratory of Analytical Chemistry for Life Science, School of Chemistry & Chemical Engineering, Nanjing University, Nanjing, China. [2]Key Laboratory of Mesoscopic Chemistry of Ministry of Education, Institute of Theoretical and Computational Chemistry, Nanjing University, Nanjing, China. [3]National Laboratory of Solid Microstructures and Collaborative Innovation Center of Advanced Microstructures, College of Engineering and Applied Science, Nanjing University, Nanjing, China. [4]MOE Key Laboratory of Materials and Surface Technology, School of Materials Science and Engineering, Xihua University, Chengdu, China. [5]Interdisciplinary Research Centre, School of Mechanical Engineering, Shanghai Jiao Tong University, Shanghai, China. ✉e-mail: yangt@sjtu.edu.cn; qdshen@nju.edu.cn

A high electric field is often required in the practical application of electrocaloric refrigeration, which can lead to electronic crosstalk and even damage the devices[10], thereby reducing long-term stability and service life. Consequently, significant efforts aim to achieve a satisfactory cooling effect at the maximum supply voltage of modern chips. In recent years, with a deeper understanding of the microscopic mechanism, various strategies have emerged to improve electrocaloric performance, including electric polarization enhancement, phase transition optimization, and nano-interface regulation[11,12]. Nanofillers have been introduced into the electrocaloric polymer matrix to synergistically enhance passive and active thermal management by improving both thermal conductivity and electrically-driven cooling performance[13]. Among these, two-dimensional (2D) materials have recently been utilized for passive thermal management[14] due to their high in-plane thermal conductivity. Furthermore, their unique physical structure and tunability make them highly promising for applications in electronics, optoelectronics, energy storage, catalysis, biomedicine, and sensor technologies[15,16]. In related research, the thermal conductivity of the electrocaloric polymers has been enhanced by incorporating two-dimensional inorganic insulators, such as boron nitride (BN) nanosheets, known for their high thermal conductivity, However, this integration has not led to an improvement in electrocaloric performance[17].

Here, we incorporate a two-dimensional polyamide (2DPA)[18] into the matrix of electrocaloric terpolymer P($VDF_{64.6}$-$TrFE_{26.2}$-$CFE_{9.2}$) (P3), and unexpectedly discover that the unique 2D confined structure and hydrogen bond of 2DPA spontaneously induce the transition of polar conformation in terpolymer. The cooling efficiency is regulated by the microstructure formed through intermolecular interactions. The effects of polarity induction are observed using micro-spectroscopy, crystallography, and dielectric spectroscopy. Notably, the electrocaloric (EC) performance is remarkably enhanced under an electric field as low as 40 MV m^{-1}, indicating that these polar microstructures play a crucial role in ECE, significantly reducing the driving energy required for EC refrigeration. The introduction of two-dimensional materials into EC refrigeration systems is of great significance for exploring performance controlled by microstructures.

Results and discussion

Multi-point polarized electrocaloric polymer with high ECE

The fabrication and microstructure of the 2DPA and P3 composite films were comprehensively depicted in Fig. 1a. During the assembly process, 2DPA was seamlessly integrated into the terpolymer matrix due to the co-solubility of the system. The interaction between the amide hydrogen bonds in 2DPA and the carbon-fluorine dipoles in P3 disrupted the typical interaction present in the pure terpolymer, effectively restricting the P3 chains in a two-dimensional framework. To shed light on how 2DPA influences electrocaloric molecular conformations, we employed both ab initio molecular dynamics (AIMD) and density functional theory (DFT) to simulate the theoretical processes depicted in Fig. 1b, c. In geometry optimizations, the 2DPA model system was considered as an environment that affected the conformational change of terpolymers. Under the 2D restricted region and hydrogen bond, 2DPA promoted the transformation of P3 to polar conformation, with the terpolymer chains extending along the 2D framework. The porous structure led to the coexistence of various polar microstructures within the system, resulting in the random distribution of polar conformation sites. Therefore, it was hard to form long-range polar conformation. We used different placement models, such as positioning the P3 molecular chains on two-dimensional skeletons or within pores, to further verify the randomness of the induction sites, as shown in Supplementary Fig. 2. Subsequently, we calculated the interaction and interfacial binding energy between P3 molecular chains with different polar conformations and 2DPA[19]. As the polarity of P3 chains increased, the interaction between its polar conformation (TTTT or T_3GT_3G') and 2DPA become more stable. On the contrary, the non-polar conformation (TGTG') had no attraction (Fig. 1d). Therefore, from the perspective of energy stability, 2DPA tended to induce multi-polar structural systems.

Compared with the long-range all-trans conformation (TTTT), the multi-site polar conformation results in a more evenly distributed system energy, which is favorable for the phase transition process and brings surprising electrocaloric performance.

To support this viewpoint, we characterize the ECE of the sample using an in-situ calibrated calorimetry system. The related calculation methods and parameters are shown in Supplementary Section 3. The experimental data indicated that 2DPA enhanced the ECE, which was mainly related to the dispersion of 2DPA and its interaction with P3. Specifically, composite materials containing 10% 2DPA exhibited an impressive ΔS that reached 24.2 $J{\cdot}kg^{-1}{\cdot}K^{-1}$ at 60 $MV{\cdot}m^{-1}$ and the ΔT was 4.8 K (Fig. 1e, f), marking a substantial 200% improvement compared to the pure terpolymer. It was worth noting that electrocaloric strength ($\Delta S/\Delta E$) in Supplementary Fig. 4d of 2DPA composite films responded rapidly to change in the external electric field within the range of 20–40 $MV{\cdot}m^{-1}$. A large conformational rearrangement occurred inside the molecule in this electric field interval. To further explore how the 2DPA-induced polar fraction enhances the ECE, we performed phase-field simulations on the electrocaloric performance of the material, with detailed methodology and results provided in Supplementary Section 3.2. Based on the time-dependent Ginzburg-Landau kinetics of the field-induced structural response, the simulation indicated that the electrocaloric entropy change is significantly enhanced in the vicinity of the terpolymer/2DPA interfaces, as shown in the inset of Fig. 1e. The simulated spatial average of the entropy change increased from 15.68 $J{\cdot}kg^{-1}{\cdot}K^{-1}$ for the terpolymer to 30.8 $J{\cdot}kg^{-1}{\cdot}K^{-1}$ of the 2DPA composite, which is consistent with our experimental measurements. The phase-field simulation also reveals a local increase of field-induced polarization response near the interface. This, combined with the crystallographic phase transition observed via XRD, suggests the emergence of enhanced short-range dipole ordering upon the introduction of 2DPA into the terpolymer. The short-range polarization sites provide more motion directions for the dipole entities, induce the transition of the surrounding terpolymer from the non-polar phase to the polar phase, and reduce the energy barrier of the phase transition, thereby improving the ECE. Additionally, the integral method[20–22] was used to evaluate the coefficient of thermal performance (COP) of the EC film, as shown in Fig. 1g, the COP value of the P3 + 10% 2DPA complex was 19.9 at 40 $MV{\cdot}m^{-1}$, which was 188% higher than that of the terpolymer at room temperature. The enhanced ECE at low fields was particularly advantageous as it significantly alleviates the electron crosstalk, a common issue in high-field applications.

To visualize the temperature evolution, we employed an infrared (IR) camera to monitor the temperature variation of the EC film under the applied electric fields. Thermal conductive silicone grease (SiG) was applied to enhance the Au surface emissivity for measurement accuracy. The temperature of the SiG-coated samples was recorded via IR camera, while the ECE polymer temperatures were calculated using the Supplementary Equations (18 and 19). As shown in the inset of Fig. 1f, the 2DPA composite films exhibited a marked enhancement in cooling ΔT. Accounting for both the heating losses in the SiG coating and thermal dissipation across the polymer, gold, and SiG interfaces, the temperature variations measured via infrared thermography demonstrated good agreement with calorimetric results (see Supplementary Table 1 and Supplementary Section 3.4 for details). Based on driving models from the literature[20,23], we optimized the active area design and achieved a vertical deformation of approximately 2 mm at 70 $MV{\cdot}m^{-1}$, which can be attributed to the electrostriction[24,25] of the electroactive polymer (Supplementary Section 4). These results demonstrate significant potential for developing self-driven electric refrigeration devices.

https://doi.org/10.1038/s41467-024-55726-5

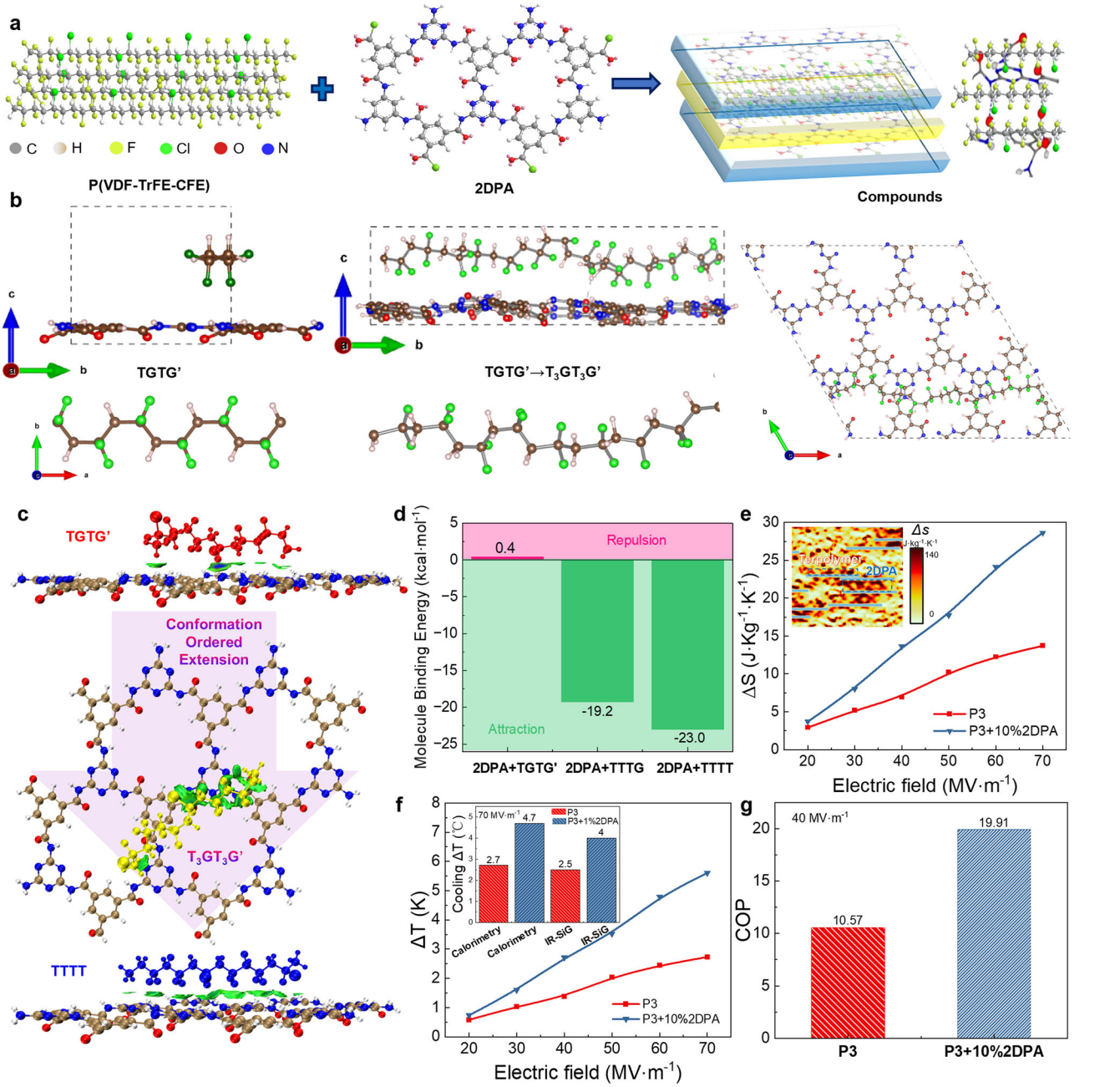

Fig. 1 | Polar multi-entropy electrocaloric effect (ECE) of P(VDF-TrFE-CFE) (P3) assisted by two-dimensional polyamide (2DPA): molecular assembly and performance. a Schematic illustration of molecular micro-assembly between P3 and 2DPA during preparation. **b** Random polarization sites of the P3 conformation simulated by AIMD under 2DPA induction. **c** Schematic diagram of the molecular interactions between 2DPA and fluoropolymer with different polar conformations (TGTG', T_3GT_3G', TTTT). **d** Quantitative statistics of intermolecular interaction energies shown in (**c**). **e** Entropy change ΔS, inset: spatial distribution from phase-field simulation of 10% 2DPA composites. **f** Temperature change ΔT, inset: comparison between infrared thermography and in-situ calorimetric measurements. **g** Coefficient of thermal performance (COP) of 2DPA-induced P3 electrocaloric films.

Compatibility and polar conformations

To validate the theoretical assumptions, we investigated the distribution and morphology of 2DPA within the P3 matrix (Fig. 2) using infrared photoinduced force microscopy (IR-PiFM). As depicted in Fig. 2a, the topography of the 10% 2DPA composite exhibited a crystalline structure similar to P3 films. The IR-PiFM provided nanoscale infrared chemical maps by combining wavelength-tunable lasers with AFM to detect microstructures[26]. We identified 1750 cm^{-1} and 1110 cm^{-1} as probing wavelengths, corresponding to the characteristic absorption peaks of 2DPA and terpolymer, respectively (Fig. 2c). The chemical spectrum of 2DPA correlated well with the brighter (harder) regions in the phase diagram (Fig. 2b, d, e), consistent with the planar rigidity of 2DPA. These brighter regions extended throughout the crystal cluster rather than being localized to specific areas, suggesting that 2DPA was incorporated into the crystallization process. Analysis of the chemical spectra of 2DPA and P3 (Fig. 2f) revealed only changes in overall signal intensity, with no significant shifts in characteristic peak positions. The results demonstrated that there was no obvious phase separation structure between the two components, instead, they exhibited excellent compatibility and uniformly participated in crystal

https://doi.org/10.1038/s41467-024-55726-5

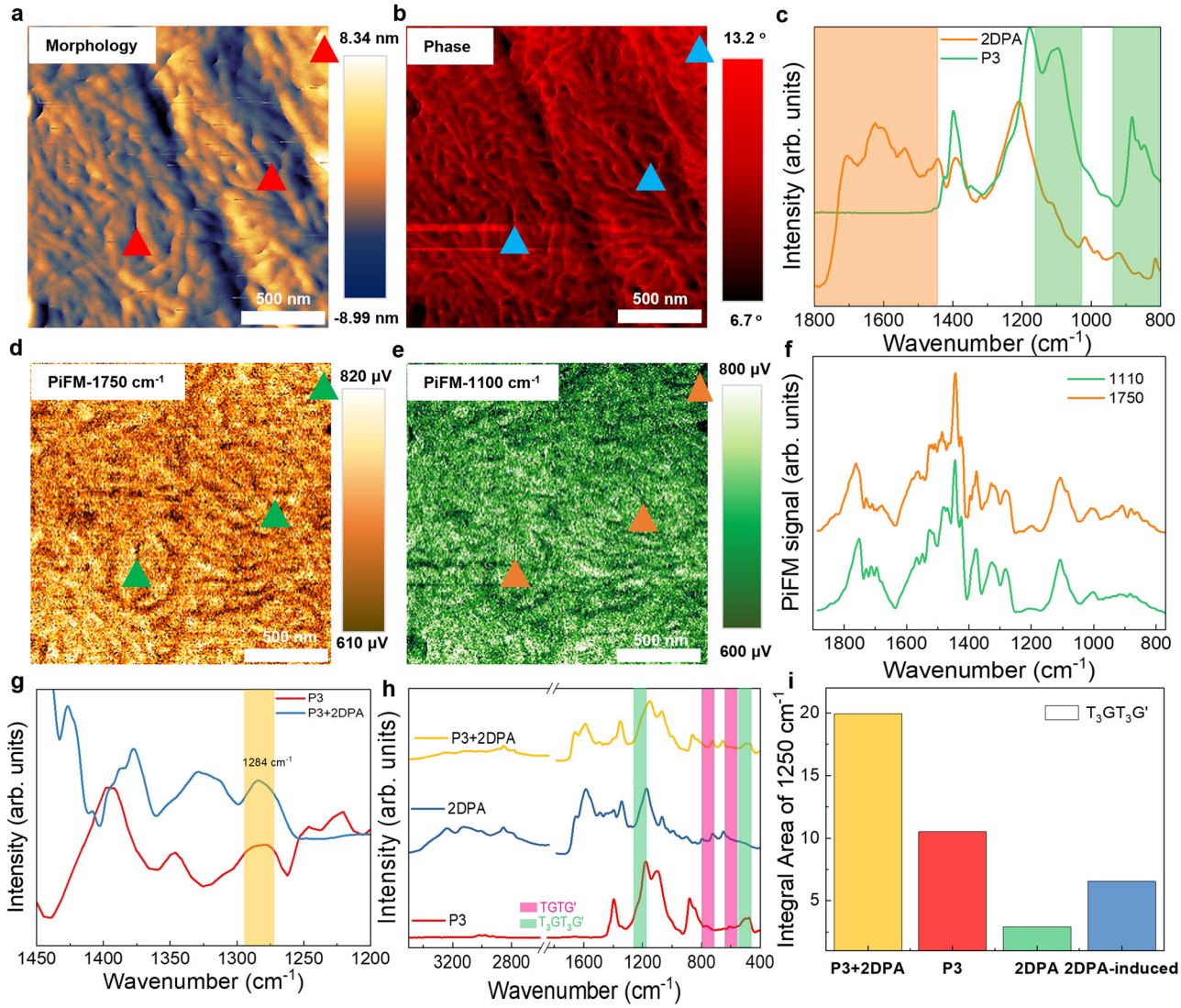

Fig. 2 | Microscopic conformation analysis of 2DPA-induced multi-entropy electrocaloric film. a, **b** IR-PiFM measurements of P3 + 10% 2DPA films: topography and phase images. **c** Infrared absorption spectra of 2DPA and P3. **d**, **e** Corresponding AFM-IR chemical maps under irradiation at 1750 cm^{-1} and 1110 cm^{-1}. **f** Normalized full IR spectrum of corresponding AFM-IR chemical maps (**d**: 1750 cm^{-1}, **e**: 1110 cm^{-1}). **g** Normalized full IR spectrum of corresponding AFM-IR chemical maps for P3 and P3 + 10% 2DPA films. **h** Infrared spectra of P3, 2DPA, and P3 + 2DPA composite. **i** Peak fitting at 1250 cm^{-1} and quantification of conformations contributed by 2DPA in the composite film.

formation. This molecular-level homogeneity is crucial for maintaining consistent electrocaloric film performance, as it alleviates electrical instability and addresses industrialization challenges caused by the compositional heterogeneity.

To investigate the role of 2DPA in the system, PiFM signals from P3 films were compared with those from the 10% 2DPA composite films. The composite film exhibited a characteristic absorption peak at 1284 cm^{-1}, indicating the presence of all-trans conformation (Fig. 2g), which confirmed enhanced polar ordering. The conventional infrared spectra revealed a diminished intensity of the non-polar TGTG′ conformational peak, concurrent with enhancement of the polar T_3GT_3G' conformation (Fig. 2h). Further evidence of T_3GT_3G' conformation enhancement was observed at 500 cm^{-1} in temperature-dependent infrared spectrum (Supplementary Fig. 16). Due to the considerable overlap between the characteristic absorption peaks of 2DPA and P3, we performed a fitting of the T_3GT_3G' conformation peak at 1250 cm^{-1}. The introduction of 2DPA in the composite system increased the proportion of T_3GT_3G' conformation by approximately 32.5% (Fig. 2i).

Phase structural analysis

We conducted a series of X-ray spectroscopy analyses to understand how 2DPA affects crystallization and its correlation with ECE. The results of small-angle X-ray scattering (SAXS) are shown in Fig. 3a–c. The two-dimensional diffraction patterns and intensity distribution curves demonstrated that incorporating 2DPA resulted in a notable decrease in scattering intensity and a gradual reduction in electron density fluctuations (Δp), indicating a weakening of the long-period ordered structure within the system. This suggested that the introduction of 2DPA reduces the inhomogeneity of each structural phase in terpolymer, thereby lowering the energy barrier for phase transitions in electrocaloric polymer. With increasing 2DPA content, the scattering peak moved to lower angles; for instance, the peak center moved from 45 nm to 51 nm in P3 + 10% 2DPA films. This shift might originate from the coexistence of multiple polar phases induced by the two-dimensional structure and the straightening of polar chain segments[27], enlarging the long-period structure. According to the Porod law, semi-crystalline polymers are characterized by their

https://doi.org/10.1038/s41467-024-55726-5

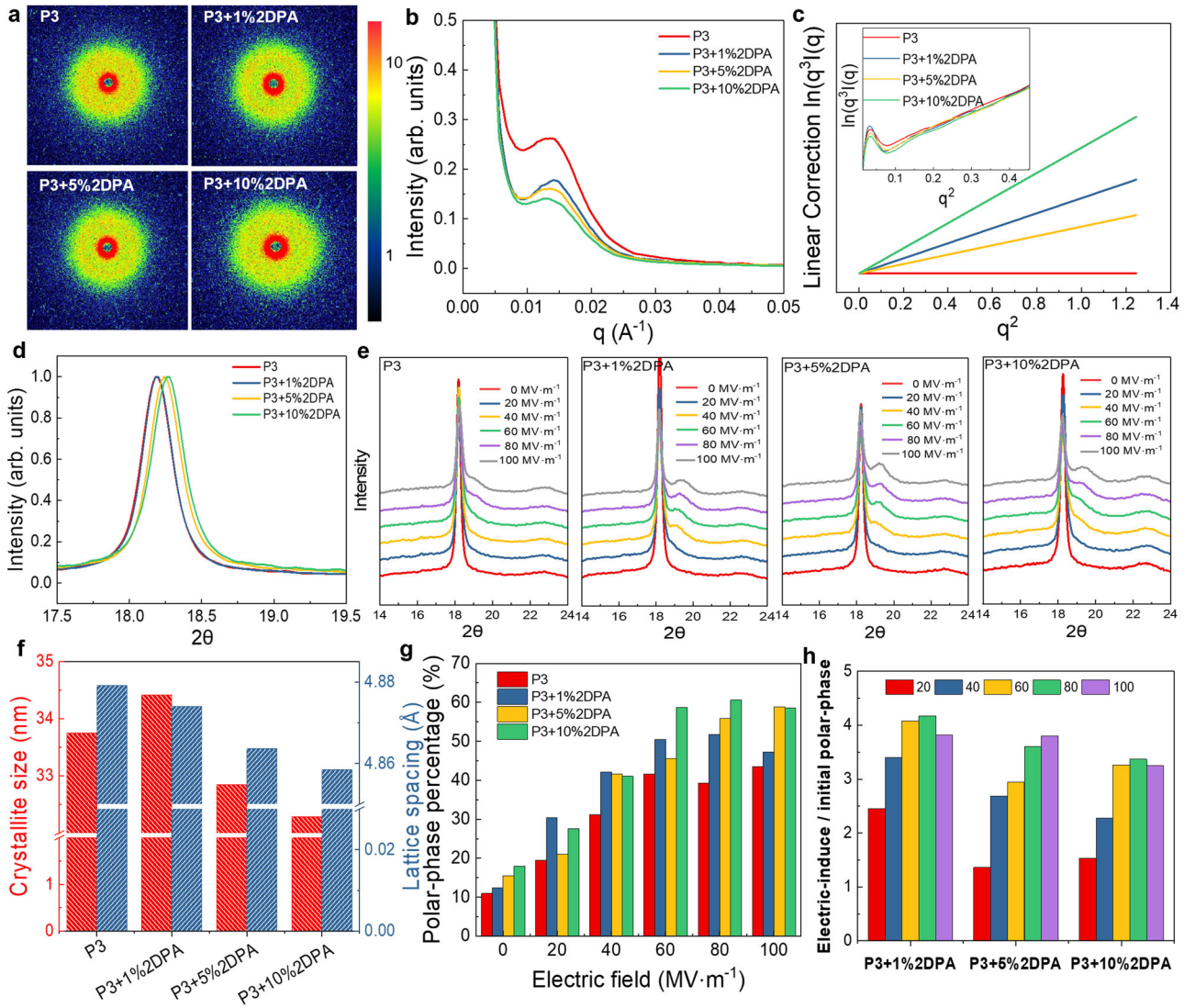

Fig. 3 | Structural evolution and phase transitions in 2DPA-induced multi-entropy electrocaloric Films. a, **b** Small-angle X-ray scattering (SAXS) patterns and curves of electrocaloric films with different 2DPA feeding ratios. **c** Calibrated Porod law deviation curve. **d** Normalized wide-angle X-ray diffraction (WAXD) data. **e** In-situ WAXD measurements of P3 and 2DPA composite under applied electric fields. **f** Calculated average crystallite sizes and lattice spacings. **g** Electric field-induced enhancement of polar phases in the crystalline regions of P3 and 2DPA composites. **h** Ratio of enhanced polar phases to initial polar crystal phase.

amorphous components and interfaces with inhomogeneous electrons or thermal density fluctuations, which do not strictly follow the $I(q) \propto q^3$ relationship, resulting in deviations[28,29]. The Porod constant in small-angle scattering is related to the interface surface area of the material, and its change trend is influenced by the composite ratio and dispersion of 2DPA. After calibrating for the pure terpolymer, the introduction of 2DPA exhibited a positive deviation. The trend of varying composite ratios showed a positive correlation with ECE performance, further supporting the enhanced polarization-induced ECE at the interface observed in the phase-field simulations.

We believe that the introduction of 2DPA creates additional polar regions within the terpolymer conformation, which will reduce the energy required for the polarity transitions. This, in turn, facilitates a more energy-efficient β-phase transition process in the ECE. The in-situ wide-angle X-ray diffraction (WAXD) was performed to explore the electric-field-induced phase transitions in the polymeric materials (Fig. 3d–f). Under the zero field conditions, the 2DPA promoted the formation of ordered polar phases with increasing concentration. The enhanced molecular bonding resulted in reduced crystal plane spacing. A notable increase in grain size was observed in P3 + 1% 2DPA films, which indicated that the low doping ratio promotes the development of microstructures adjacent to the polar phase, facilitating the crystallization process. Compared to pure terpolymer, the 2DPA composite exhibited enhanced polar crystalline phase induction at lower field strengths. At 40 MV·m^{-1}, the P3 + 1% 2DPA electrocaloric film could induce a characteristic peak at approximately 19.2°, which represented the presence of field-induced polar phase-like (all trans, TTTT) conformations in Fig. 3e.

Peak fitting analysis of the diffraction patterns and quantitative assessment of polar crystalline phases shown in Fig. 3g, h, it was observed that 2DPA promoted the polar phase formation from the initial state. The polar region proportion increased with 2DPA doping concentration, reaching 11%, 12.4%, 15.5%, and 18%, respectively. The proportion of polar crystalline phase in terpolymer increased by 30% at 80 MV·m^{-1}, while the polar crystalline phase transitions of P3 + 1% 2DPA, P3 + 5% 2DPA, and P3 + 10% 2DPA accounted for 38%, 40%, and 43%, respectively, confirming that increased polar conformation facilitates phase transition (Supplementary Fig. 17). Under equivalent electric field conditions, the P3 + 10% 2DPA composite exhibited a polar phase ratio approximately 1.5 times that of P3. This result aligns

https://doi.org/10.1038/s41467-024-55726-5

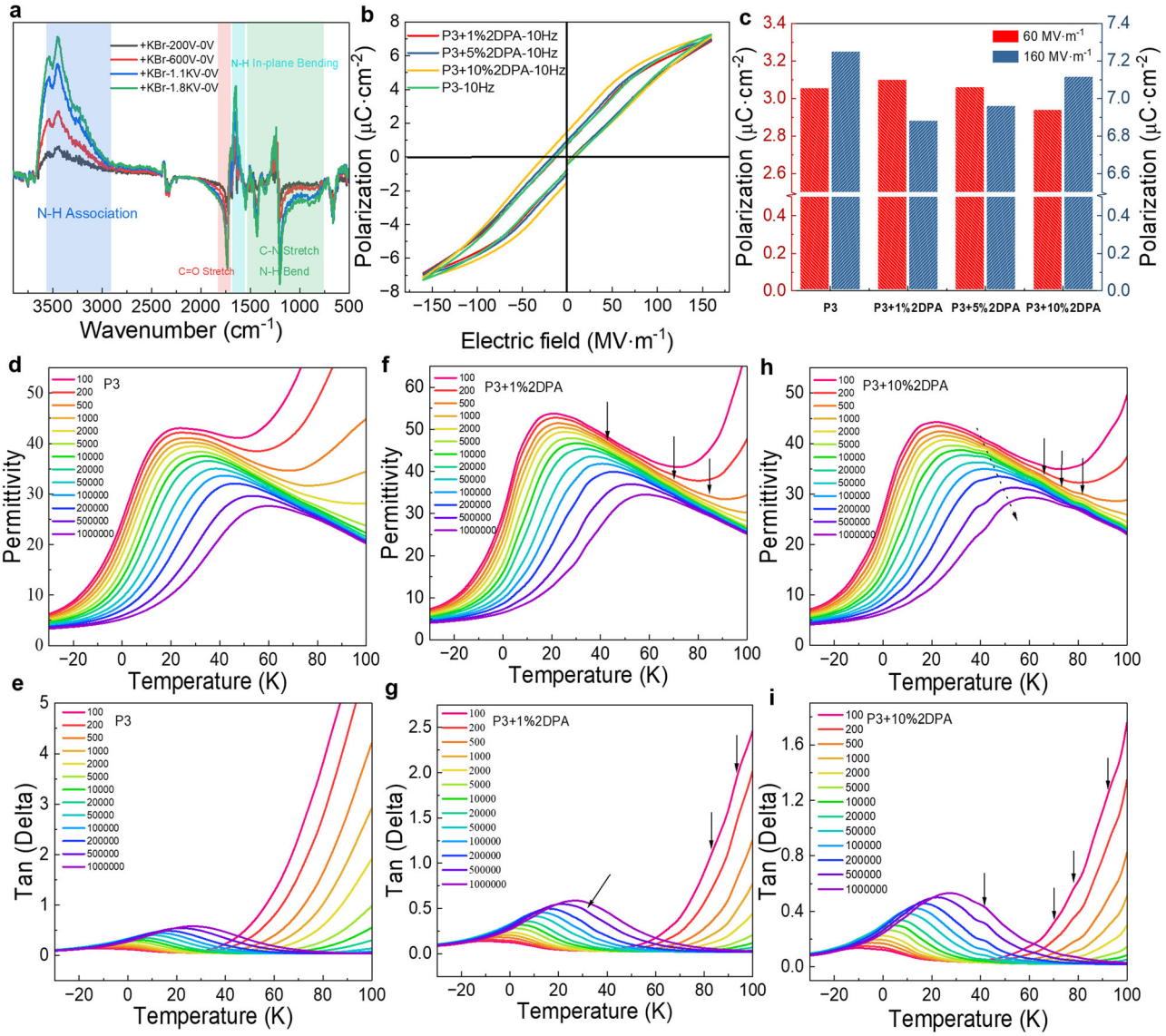

Fig. 4 | Electrical polarization and dielectric response of 2DPA composite electrocaloric polymer film. a Infrared differential spectrum of 2DPA under varying electric fields. **b** Bipolar polarization-electric field loops. **c** Maximum polarizations under electric fields of 60 and 120 MV·m^{-1}. **d**–**i** Temperature-dependent dielectric permittivity and loss of the P3 polymer and 2DPA composites. The arrows indicate the polar phases induced by 2DPA.

with the results of the β coefficient calculated by Devonshire phenomenological theory in phase field simulation. (See Supplementary Section 8.1 for details). Moreover, it exhibited the maximal polar phases proportion at 60 MV·m^{-1}, approaching 60%, maintaining stability at higher field strengths. The low-field polar phase emergence was attributed to the multi-point polar conformation induction, which balanced the system energy similar to polar nuclei-mediated crystal growth. Furthermore, reduced grain size lowered the energy barrier for non-polar grain disruption, promoting phase transitions.

Polarization and dielectric analysis

Variable-field infrared spectroscopy (Fig. 4a) revealed molecular structural modifications in 2DPA during electrical polarization. Significant spectral changes were observed, particularly in amide hydrogen bond-associated peaks. When the applied electric field was orthogonal to the infrared detection axis, the N-H bond characteristic peaks increased, while covalent bonds (such as C = O and C-N) peaks showed inverse enhancement. This behavior originated from the molecular vibration coupling or energy transfer within the amide bond. Furthermore, the 2DPA molecular absorption peak enhancement demonstrated linear correlation with field strength. This mechanism was conducive to synergistic dipolar activity within the material, initiating a cascade effect in the composite films that enhanced coordinated dipolar motion. These observations illuminate the molecular-level interactions governing ECE, where field-induced structural alignment provides mechanistic insights into composite material behavior.

In the polarization-electric field (P-E) loops (Fig. 4b, c), polarization decreased progressively with increasing 2DPA content at low field strengths. According to the Landau–Devonshire phenomenological theory, the isothermal entropy change ΔS is proportional to both β and the square of polarization, the β value is related to the number of dipole entities and the polarization directions. Supplementary Fig. 19 confirms that 2DPA-induced polarization sites enhance the ECE by providing more dipolar motion pathways. The short-range polarity region shows high dynamic, randomness, and disorder on the whole[30], which cannot enhance the overall polarization. However, the polarization was markedly enhanced under

high electric fields, which implies that 2DPA actively participated in the polarization mechanism at elevated field strengths. The temperature-dependent dielectric spectra of P3 film and 2DPA composite film were presented in Fig. 4d–i. Pre-annealing measurements of the 1% 2DPA electrocaloric film showed a characteristic peak at 73 °C, corresponding to dual loss spectrum peaks, suggesting two similarly polar structures (Supplementary Fig. 20). This observation was consistent with the XRD results, where similar structures facilitated crystallization in P3 + 1% 2DPA films. In higher 2DPA content composites, the dispersed polar conformation inhibited crystallization and growth, preventing long-term polar structure formation. Post-annealing treatment at 120 °C revealed multiple minor polar peaks. Particularly, the 10% 2DPA composite film exhibited four frequency-stable distinct peaks, coexisting in both the dielectric permittivity and loss spectra, indicating the formation of numerous short-range nanoscale polar phases[31,32]. These initially undetectable grains became observable post-annealing. The introduction of 2DPA shifted the P3 conformation towards short-range polarity, resulting in the emergence of diverse regional polar phases. These microstructure modifications reflect 2DPA's modulation of the P3 matrix micro-environment, highlighting the intricate interplay between material composition and electrocaloric properties.

By introducing a two-dimensional polyamide as a spatially confined structure template, we effectively guided the ordered conformational transformation of the electrocaloric polymer in the two-dimensional plane, thereby enhancing its ECE. Through a combination of various experimental and theoretical approaches, we thoroughly explored the impact of 2DPA on the microstructure of electrocaloric polymer. The porous two-dimensional amide structure facilitated the formation of multi-site polar microstructures, increasing the system's conformational complexity and lowering the energy barrier for phase transitions between conformations. This study provides a crucial foundation for the development of energy-efficient and environmentally friendly cooling technologies. Moreover, it opens up additional possibilities for applying advanced two-dimensional materials in various fields.

Methods

Materials

Melamine (99%), 1,3,5-benzenetricarboxylic acid chloride (98%), *N*-methyl-2-pyrrolidone (99.5%), pyridine (99.5%), ethyl alcohol (≥99.7%), acetone (≥99.5%), and *N, N*-dimethylformamide (>99.9%) were purchased from Aladdin. The terpolymer P($VDF_{64.6}$-$TrFE_{26.2}$-$CFE_{9.2}$) (P3) powders were purchased from Piezotech in Arkema, France.

Synthesis of two-dimensional polyamide (2DPA)[18]

Melamine (126 mg, 1 mmol) and 1,3,5-benzenetricarboxylic acid chloride (265 mg, 1 mmol) were added to a 40 mL bottle containing a stir bar, followed by 9 ml of *N*-methyl-2-pyrrolidone and 1 mL of pyridine. The mixture was carried out at room temperature for 16 h. the whole reaction mixture became a gel. This gel was poured into ethyl alcohol (80 mL) and sonicated for 30 min, followed by filtration or centrifugation. The precipitate was washed with deionized H_2O (80 mL) and acetone (80 mL). The product was dried under vacuum at 100 °C for 16 h to yield a yellow powder (228 mg, 81%).

Preparation of the ECE films

The polymer films were prepared via solution-casting methods according to the literature[25]. The terpolymer powder was dissolved in N, N-dimethylformamide to prepare a 6 wt% solution. A predetermined amount (1%, 5%, and 10%) of 2DPA was added to form a complex solution. After stirring for 12 h, the solution was filtered through a glass fiber syringe filter with 0.7 μm pore size. The filtered solution was cast onto a quartz plate and dried at 60 °C for 8 h, and subsequently peeled off from the plates, the obtained films were annealed in a vacuum oven at 120 °C for 10 h to improve the crystallinity. The resulting film thickness was approximately 20 μm and could be tuned by varying the concentration of the solutions and the area of the plates.

Qualitative characterization of 2DPA

The synthesis of two-dimensional polyamide was determined by the characteristic peaks of Fourier transform infrared spectroscopy (FTIR, Nicolet iS10, Thermo Fisher Scientific) and liquid nuclear magnetic resonance (BRUKER AVANCE III 400 MHz). The two-dimensional planar structure was confirmed by atomic force microscopy (AFM, Bruker Icon) and transmission electron microscopy (TEM, JEM-2100). Additional details are available in Supplementary Fig. 1.

DFT calculation

The intermolecular interactions between P3 and 2DPA model system were calculated at B3LYP-D3(BJ)/6-311 + G(d,p) level. An independent gradient model based on Hirshfeld partition (IGMH) analysis[19] was employed in the visual descriptions of the intermolecular interactions. All geometry optimizations and intermolecular interaction calculations at TDDFT level with B3LYP functional were performed by the GAUSSIAN16 programs (Gaussian 16, Revision C.01)[33]. The IGMH analysis was conducted by the Multiwfn-3.8 program[34]. The visualizations of all the structures and intermolecular interactions were drawn by the VMD-1.9.3 program[35].

ECE performance

The ECE heat calibration and the electrocaloric stack cooling and heating heat flow were captured by the heat flux sensor (HFS-4, OMEGA). The high voltage was generated by a high-voltage power module (LNC 30000, Heinzinger). The low-voltage system was produced by a high-precision digital source meter (B2902A, KEYSIGHT). The phase field model was used to study the relaxor ferroelectric phase transition at the 2DPA interface. The surface temperature change of samples was recorded in real-time by an infrared thermographic camera (226 s, FOTRIC). More details about the measurement of ECE can be found in Supplementary Section 4.

Structural characterization

The morphology and conformational evolution of the P3 polymer after the introduction of 2DPA were investigated using IR Photo-induced Force Microscopy (IR-PiFM) and the Langmuir-Blodgett (LB) film technique. The IR-PiFM system (Molecular Vista Inc., VistaScope) was used to observe the changes, while the LB film technique was employed to assemble the P3 molecular layer on the two-dimensional polyamide, allowing for detailed analysis of the microscopic conformational changes. WAXD and SAXS characterizations were employed to monitor the structural evolution under electric fields. The crystal structure and its change under an electric field were analyzed by X-ray diffractometer (XRD, Bruker D8 ADVANCE). Two-dimensional SAXS patterns and related data were collected using Nanostar SAXS. The crystallinity and crystal size were evaluated by differential scanning calorimetry (DSC X3, Mettler-Toledo, Switzerland).

Electrical measurement

All the films for electrical tests were sputtered with gold electrodes for 600 s with a typical thickness of 150 nm, and the diameter of the upper and bottom electrodes was all set as 10 mm.

The dielectric properties were measured by broadband dielectric and impedance analyzer (Concept 80, Novocontrol Technologies, Germany). The ambient temperature was controlled by a digitally oven equipped with a nitrogen tank. The temperature ramp was set to

4 K·min^{-1} from 100 Hz to 1 MHz. Ferroelectric hysteresis loops were characterized by Ferroelectric Test Systems (Premier II, Radiant Technologies, USA) throughout a frequency range of 10 Hz to 1000 Hz with a rising electric field intensity (10–200 MV·m^{-1}).

Data availability

All data that support the findings of this study are included in the manuscript and Supplementary Information. All data is available from the corresponding authors on request.

References

1. Cappello, F. et al. Toward exascale resilience: 2014 update. *Supercomput. Front. Innov.: Int. J.* **1**, 5–28 (2014).
2. Platini, M., Ropars, T., Pelletier, B. & De Palma, N. CPU overheating prediction in HPC systems. *Concurr. Comput.: Pract. Exp.* **33**, e6231 (2021).
3. Shi, J. et al. Electrocaloric cooling materials and devices for zero-global-warming-potential, high-efficiency refrigeration. *Joule* **3**, 1200–1225 (2019).
4. Liu, Y., Scott, J. F. & Dkhil, B. Direct and indirect measurements on electrocaloric effect: recent developments and perspectives. *Appl. Phys. Rev.* **3**, 031102 (2016).
5. Ma, R. et al. Highly efficient electrocaloric cooling with electrostatic actuation. *Science* **357**, 1130–1134 (2017).
6. Bai, P. et al. An active pixel-matrix electrocaloric device for targeted and differential thermal management. *Adv. Mater.* **35**, 2209181 (2023).
7. Bai, P. et al. A highly efficient cascade electrocaloric cooling tube with enhanced temperature change by sawtooth voltage. *Materials* **1**, 100001 (2023).
8. Wang, H. et al. Self-actuating electrocaloric cooling fibers. *Adv. Energy Mater.* **10**, 1903902 (2020).
9. Wang, Z. et al. Self-sustaining personal all-day thermoregulatory clothing using only sunlight. *Science* **382**, 1291–1296 (2023).
10. Jahani, S. et al. Controlling evanescent waves using silicon photonic all-dielectric metamaterials for dense integration. *Nat. Commun.* **9**, 1893 (2018).
11. Zheng, S. et al. Colossal electrocaloric effect in an interface-augmented ferroelectric polymer. *Science* **382**, 1020–1026 (2023).
12. Qian, X. et al. High-entropy polymer produces a giant electrocaloric effect at low fields. *Nature* **600**, 664–669 (2021).
13. Li, M.-D. et al. Thermal management of chips by a device prototype using synergistic effects of 3-D heat-conductive network and electrocaloric refrigeration. *Nat. Commun.* **13**, 5849 (2022).
14. Song, H. et al. Two-dimensional materials for thermal management applications. *Joule* **2**, 442–463 (2018).
15. Wang, L. et al. Emerging synthesis strategies of 2D MOFs for electrical devices and integrated circuits. *Small* **18**, 2201642 (2022).
16. Evans, A. M. et al. Thermally conductive ultra-low-k dielectric layers based on two-dimensional covalent organic frameworks. *Nat. Mater.* **20**, 1142–1148 (2021).
17. Han, D. et al. Molecular interface regulation enables order-disorder synergy in electrocaloric nanocomposites. *Joule* **7**, 2174–2190 (2023).
18. Zeng, Y. et al. Irreversible synthesis of an ultrastrong two-dimensional polymeric material. *Nature* **602**, 91–95 (2022).
19. Lu, T. & Chen, Q. Independent gradient model based on Hirshfeld partition: a new method for visual study of interactions in chemical systems. *J. Comput. Chem.* **43**, 539–555 (2022).
20. Defay, E., Crossley, S., Kar-Narayan, S., Moya, X. & Mathur, N. D. The electrocaloric efficiency of ceramic and polymer films. *Adv. Mater.* **25**, 3337–3342 (2013).
21. Zhao, Y., Hao, X. & Zhang, Q. A giant electrocaloric effect of a $Pb_{0.97}La_{0.02}(Zr_{0.75}Sn_{0.18}Ti_{0.07})O_3$ antiferroelectric thick film at room temperature. *J. Mater. Chem. C.* **3**, 1694–1699 (2015).
22. Zhao, Q. et al. Highly efficient and giant negative electrocaloric effect of a Nb and Sn co-doped lead zirconate titanate antiferroelectric film near room temperature. *RSC Adv.* **9**, 34114–34119 (2019).
23. Zhu, Y. et al. Operando investigation of the molecular origins of dipole switching in P(VDF-TrFE-CFE) terpolymer for large adiabatic temperature change. *Adv. Funct. Mater.* **34**, 2314705 (2024).
24. Chen, X., Zhu, W., Rattner, A. S. & Zhang, Q. M. A self-actuated electrocaloric polymer heat pump design exploiting the synergy of electrocaloric effect and electrostriction. *J. Phys.: Energy* **5**, 024009 (2023).
25. Chen, X. et al. Relaxor ferroelectric polymer exhibits ultrahigh electromechanical coupling at low electric field. *Science* **375**, 1418–1422 (2022).
26. Diem, M., Romeo, M. J., Boydston-White, S. & Matthäus, C. in *Spectrochemical Analysis Using Infrared Multichannel Detectors*, (ed. Bhargava, R. & Levin, I. W.) 189–203 (Blackwell Publishing Ltd Editor(s), 2005).
27. Liu, C. et al. Low voltage–driven high-performance thermal switching in antiferroelectric $PbZrO_3$ thin films. *Science* **382**, 1265–1269 (2023).
28. Chu, B. & Hsiao, B. S. Small-angle X-ray scattering of polymers. *Chem. Rev.* **101**, 1727–1762 (2001).
29. Li, X.-Y., Ding, J.-J., Liu, Y.-P. & Tian, X.-Y. A new small-angle X-ray scattering model for polymer spherulites with a limited lateral size of the lamellar crystals. *IUCrJ* **6**, 968–983 (2019).
30. Hirota, K., Ye, Z. G., Wakimoto, S., Gehring, P. M. & Shirane, G. Neutron diffuse scattering from polar nanoregions in the relaxor $Pb(Mg_{1/3}Nb_{2/3})O_3$. *Phys. Rev. B.* **65**, 104105 (2002).
31. Zhang, S. et al. in *Frontiers of Ferroelectricity: A Special Issue of the Journal of Materials Science* (eds Sidney B. Lang & Helen L. W. Chan) 271–280 (Springer US, 2007).
32. Liu, J., Zhou, Y., Hu, X. & Chu, B. Flexoelectric effect in PVDF-based copolymers and terpolymers. *Appl. Phys. Lett.* **112**, 232901 (2018).
33. Gaussian 16 Rev. C.01. https://gaussian.com/citation/. (Wallingford, CT, 2016)
34. Lu, T. & Chen, F. Multiwfn: a multifunctional wavefunction analyzer. *J. Comput. Chem.* **33**, 580–592 (2012).
35. Humphrey, W., Dalke, A. & Schulten, K. VMD: visual molecular dynamics. *J. Mol. Graph.* **14**, 33–38 (1996).

Acknowledgements

Q.-D.S. acknowledges the support of National Key Research and Development Program of China (2020YFA0711504), National Natural Science Foundation of China (Nos. 22175085, 52473133, and 21875101), the Fundamental Research Funds for the Central Universities (2023300318 and 2024300479), the Nanjing University Integrated Research Platform of the Ministry of Education - Top Talents Program, and Engineering Research Center of Photoresist Materials of the Ministry of Education. We thank X. Chen at Shanghai Jiao Tong University for the inspiring discussion.

Author contributions

F.W. and Q.-D.S. conceived the experiments. F.W. carried out the sample preparation and characterization and wrote the manuscript. M.-D.L. and X.-L.W. assisted with the experiment. Z.-Y.W. and W.L. performed the density functional theory (DFT). Y.-R.L. and Y.-R.Y. conducted ab initio molecular dynamics (AIMD), T.-N.Y. completed the establishment of the phase-field model and related calculations. F.W. and Q.-D.S. conducted mechanism discussion, and article conceptualization. All authors analyzed and interpreted the data.

Competing interests

The authors declare no competing interests.

Additional information

Supplementary information The online version contains supplementary material available at https://doi.org/10.1038/s41467-024-55726-5.

Correspondence and requests for materials should be addressed to Tiannan Yang or Qun-Dong Shen.

Peer review information *Nature Communications* thanks Veronika Kovacova and the other, anonymous, reviewer(s) for their contribution to the peer review of this work. A peer review file is available.